

# Evaluation of Under Sea-ice Phytoplankton Blooms in the Fully-Coupled, High-Resolution Regional Arctic 2 System Model 3

Marina Frants<sup>1</sup>, Wieslaw Maslowski<sup>1</sup>, Robert Osinski<sup>2</sup>, Nicole Jeffery<sup>3</sup>, Meibing Jin<sup>4</sup>, and Jaclyn Clement Kinney<sup>1</sup>

<sup>1</sup>Naval Postgraduate School

<sup>2</sup>Institute of Oceanology Polish Academy of Sciences

<sup>3</sup>Los Alamos National Laboratories

<sup>4</sup>University of Alaska Fairbanks

November 21, 2022

## Abstract

In July 2011, observations of a massive phytoplankton bloom in the ice-covered waters of the western Chukchi Sea raised questions about the extent and frequency of under sea- ice blooms and their contribution to the carbon budget in the Arctic Ocean. To address some of these questions, we use the fully-coupled, high-resolution Regional Arctic Sys- tem Model to simulate Arctic marine biogeochemistry over a thirty-year period. Our re- sults demonstrate the presence of massive under sea-ice blooms in the western Arctic not only in summer of 2011 but annually throughout the simulation period. In addition, sim- ilar blooms, yet of lower magnitude occur annually in the eastern Arctic. We investigate the constraints of nitrate concentration and photosynthetically available radiation (PAR) on the initiation, evolution and cessation of under sea-ice blooms. Our results show that increasing PAR reaching the ocean surface through the sea-ice in early summer, when the majority of ice-covered Arctic waters have sufficient surface nitrate levels, is criti- cal to bloom initiation. However, the duration and cessation of under sea-ice blooms is controlled by available nutrient concentrations as well as by the presence of sea-ice. Since modeled critical PAR level are consistently exceeded in summer only in the western Arc- tic, we therefore conclude that the eastern Arctic blooms shown in our simulations did not develop under sea ice, but were instead, at least in part, formed in open waters up- stream and subsequently advected by ocean currents beneath the sea ice.

1 **Evaluation of Under Sea-ice Phytoplankton Blooms in**  
2 **the Fully-Coupled, High-Resolution Regional Arctic**  
3 **System Model**

4 **Marina Frants<sup>1</sup>, Wieslaw Maslowski<sup>1</sup>, Robert Osinski<sup>2</sup>, Nicole Jeffery<sup>3</sup>, Meibing**  
5 **Jin<sup>4</sup>, Jaclyn Clement Kinney<sup>1</sup>**

6 <sup>1</sup>Naval Postgraduate School

7 <sup>2</sup>Institute of Oceanology Polish Academy of Sciences

8 <sup>3</sup>Los Alamos National Laboratories

9 <sup>4</sup>University of Alaska Fairbanks

10 **Key Points:**

- 11 • RASM reproduces the under sea-ice phytoplankton bloom observed in the Chukchi  
12 Sea in summer 2011
- 13 • Under sea-ice phytoplankton blooms are common in the Western Arctic and they  
14 occur under a specific combination of nutrient concentration and light
- 15 • High under sea-ice chlorophyll-*a* concentrations are also common in the Eastern  
16 Arctic, but they are at least in part a result of advection from open water blooms  
17 upstream

**Abstract**

In July 2011, observations of a massive phytoplankton bloom in the ice-covered waters of the western Chukchi Sea raised questions about the extent and frequency of under sea-ice blooms and their contribution to the carbon budget in the Arctic Ocean. To address some of these questions, we use the fully-coupled, high-resolution Regional Arctic System Model to simulate Arctic marine biogeochemistry over a thirty-year period. Our results demonstrate the presence of massive under sea-ice blooms in the western Arctic not only in summer of 2011 but annually throughout the simulation period. In addition, similar blooms, yet of lower magnitude occur annually in the eastern Arctic. We investigate the constraints of nitrate concentration and photosynthetically available radiation (PAR) on the initiation, evolution and cessation of under sea-ice blooms. Our results show that increasing PAR reaching the ocean surface through the sea-ice in early summer, when the majority of ice-covered Arctic waters have sufficient surface nitrate levels, is critical to bloom initiation. However, the duration and cessation of under sea-ice blooms is controlled by available nutrient concentrations as well as by the presence of sea-ice. Since modeled critical PAR level are consistently exceeded in summer only in the western Arctic, we therefore conclude that the eastern Arctic blooms shown in our simulations did not develop under sea ice, but were instead, at least in part, formed in open waters upstream and subsequently advected by ocean currents beneath the sea ice.

**Plain Language Summary**

In July 2011, scientists conducting research in the western Arctic Ocean observed a large phytoplankton bloom under the sea-ice. Traditionally, such blooms were believed to be rare. Using our state-of-the-art Arctic system model, we were able to demonstrate that in fact, under sea-ice blooms have been occurring annually for the past several decades. In the western Arctic, under sea-ice blooms begin when sufficient sunlight penetrates through the sea-ice to the ocean, and end when nutrient concentrations become too low to sustain the phytoplankton. In the eastern Arctic, our model shows that under sea-ice blooms still occur even when there is not enough sunlight penetrating the sea-ice. From this, we conclude that phytoplankton blooms in the eastern Arctic begin in ice-free waters and are advected beneath the sea-ice by ocean currents.

**1 Introduction**

Marine phytoplankton have a strong effect on both the physical and the biological properties of the Arctic Ocean. In addition to its role in the regional carbon budget, the presence of phytoplankton alters the optical properties of sea water, affecting water temperature, mixed layer depth, upper-ocean stratification, and sea-ice cover (Manizza, Le Quere, Watson, & Buitenhuis, 2005). Phytoplankton also form the base of the marine food web, supporting a wide variety of higher trophic organisms in pelagic communities (Grebmeier, Cooper, Feder, & Sirenko, 2006; Sigler et al., 2011), while the sink of particulate organic matter produced by photosynthesis in the euphotic zone provides the main food source in benthic communities (Grebmeier & Barry, 1991).

In high-latitude environments such as the Arctic Ocean, phytoplankton growth is strongly constrained by light availability. Because light penetration into the upper ocean is attenuated by snow and sea-ice cover, it was generally believed until recently that phytoplankton growth was limited to areas of open water, with negligible growth under the sea-ice. However, under sea-ice phytoplankton blooms have been reported multiple times over the past several decades (e.g. Fortier, Fortier, Michel, and Legendre (2002); Fukuchi et al. (1989); Hill, Light, Steele, and Zimmerman (2018); Legendre, Ingram, and Poulin (1989)). In July 2011, an ICESCAPE (Impacts of Climate on EcoSystems and Chemistry of the Arctic Pacific Environment) survey observed a massive phytoplankton bloom beneath the sea ice in the northern Chukchi Sea (Arrigo et al., 2012). The phytoplank-

68 ton biomass was observed to be four times higher beneath the sea-ice than in the sur-  
 69 rounding open water. The bloom extended more than 100 km beneath the pack ice with  
 70 peak particulate organic carbon biomass located near the shelf break, underlying thick  
 71 sea ice. The species observed indicate that pelagic diatoms were dominate, with a much  
 72 smaller contribution from ice algae. The growth of this under sea-ice bloom was supported  
 73 by areas of thinner first-year ice and, particularly, by the presence of melt ponds that  
 74 allowed for greater penetration of light. Observational evidence suggests that this bloom  
 75 was not an isolated case, and that under sea-ice blooms maybe widespread on the Arc-  
 76 tic continental shelves (Arrigo et al., 2014; Lowry, van Dijken, & Arrigo, 2014)

77 The ICESCAPE observations have sparked increased interest in under sea-ice phy-  
 78 toplankton blooms. Several model studies have been performed to assess the physical  
 79 conditions that favor the development of such blooms. Palmer et al. (2014) used a 1-D  
 80 ecosystem model to demonstrate that sea-ice conditions, particularly melt pond prolif-  
 81 eration, contributed to under sea-ice bloom formation due to the enhanced light trans-  
 82 mission through melt pond-covered sea ice. A coupled ice-ocean model study by Zhang  
 83 et al. (2015) has demonstrated a link between simulated under sea-ice blooms and in-  
 84 creased light availability due to decreased snow cover; however, the model used in the  
 85 study did not include melt ponds. Horvat et al. (2017) formulated a model based on the  
 86 Sverdrup critical depth hypothesis (Sverdrup, 1953), suggesting that under sea-ice blooms  
 87 can form when melt pond fraction exceeds a critical value  $\Phi_c$ , but this study did not ad-  
 88 dress nutrient availability, which was demonstrated to be important by Zhang et al. (2015).

89 The purpose of this study is to examine the temporal and spatial evolution of under  
 90 sea-ice blooms in the fully-coupled, bio-physical, high-resolution Regional Arctic Sys-  
 91 tem Model (RASM) from 1980 to 2011. The model has been expanded to include ma-  
 92 rine biogeochemistry (mBGC) in its ocean and sea ice components, with the latter in-  
 93 cluding multiple options for melt pond representation. As such, RASM is a powerful tool  
 94 to investigate air-sea and bio-physical coupling in presence of sea ice at seasonal to multi-  
 95 decadal time scales. We first evaluate the model bio-physical skill by comparing the mod-  
 96 eled chlorophyll-*a* (chl-*a*) results against observations of the phytoplankton bloom in the  
 97 Chukchi Sea during July 3-8 2011, as reported by Arrigo et al. (2012). Next, we exam-  
 98 ine multi-decadal variability of the under sea-ice chl-*a* and nutrient distributions, as well  
 99 as photosynthetically available radiation (PAR) for three different decade-apart years  
 100 spanning the period from 1991-2011. Finally, we discuss the relative controls of light avail-  
 101 ability and nutrient supply on the initiation and evolution of under sea-ice phytoplank-  
 102 ton blooms in two selected regions of the western and eastern Arctic, and the contribu-  
 103 tion of these blooms to total primary production (PP).

## 104 2 The Regional Arctic System Model

105 RASM is a high-resolution, fully coupled atmosphere-ice-ocean-land regional model  
 106 with a domain encompassing the entire marine cryosphere of the Northern Hemisphere,  
 107 including the major oceanic inflow and outflow pathways, with mid-latitude extensions  
 108 into the North Pacific and North Atlantic oceans to account for the passage of cyclones  
 109 into the Arctic Ocean (Figure 1). The components of RASM are the Weather Research  
 110 and Forecasting (WRF) model, the Variable Infiltration Capacity (VIC) land hydrology  
 111 model with the river routing scheme (RVIC), and the Los Alamos National Laboratory  
 112 (LANL) Parallel Ocean Program (POP) and Sea Ice (CICE) Models. The model reso-  
 113 lution is 50 km for WRF and VIC, and  $1/12^\circ$  (approximately 9km) for POP and CICE.  
 114 RASM has been demonstrated to correspond well with observations in its representa-  
 115 tion of the upper-ocean physical dynamics (DuVivier et al., 2016; Hamman et al., 2017;  
 116 Roberts et al., 2015), arctic climate (Cassano et al., 2017; Hamman et al., 2017) and pro-  
 117 cesses across the coupled atmosphere-land-ocean-sea ice interface (Brunke et al., 2018).  
 118 Because this study focuses on marine biogeochemistry, only the details of POP and CICE  
 119 are further described below.

## 2.1 Physical ocean and sea-ice model

The POP and CICE configurations used in RASM are similar to the configuration in the Community Earth System Model (CESM) version 1.1 (<http://www.cesm.ucar.edu>) however, some adjustments have been made. In addition to changes needed to use it as a regional model, POP has been modified to include a subgrid-scale brine rejection parameterization of Jin, Deal, et al. (2012); Jin, Hutchins, Kawaguchi, and Kikuchi (2012), which improves vertical ocean mixing under sea ice. Along the vertical axis, the model is configured with 45 fixed-depth layers, including 7 layers in the top 42 m. The model horizontal resolution of  $1/12^\circ$  is eddy-permitting across the entire RASM domain. The combined effects of the fully coupled model, high spatio-temporal resolution and improved parameterization of sub-grid scale bio-physical processes allowed reduction of biases in physical and mBGC model outputs when compared to the coarse-resolution CESM model (Jin et al., 2018).

The CICE model (Roberts et al., 2018) in RASM is version 6, which includes, among a number of changes, the latest column package modifications (Hunke, Lipscomb, Turner, Jeffery, & Elliot, 2015, 2016). It has been configured to include mushy-layer thermodynamics (Turner & Hunke, 2015) and Elastic Anisotropic Plastic (EAP) sea ice rheology (Wilchinsky & Feltham, 2004), as well as the explicit level ice pond parameterization rather than the virtual melt ponds used in CESM. In addition, it uses new thermodynamic ocean coupling in which the basal freezing temperature is the same as the liquid phase temperature within sea ice. RASM CICE uses five ice thickness categories, divided at 0.65, 1.39, 2.47, 4.56 and 9.3 m.

The ice and ocean components are coupled using the coupler of Craig et al. (2012) with a coupling time step of 20 minutes to resolve sea ice-ocean inertial oscillations (Roberts et al., 2015)

The ocean and sea ice components were spun up for 78 model years, starting with the initial conditions of no sea-ice and the ocean at rest. During this stage of initialization, POP and CICE models were forced with CORE2 reanalysis (Large & Yeager, 2009). Initial ocean temperature and salinity fields were from Polar science center Hydrographic Climatology (PHC 3.0), (Steele, Morley, & Ermold, 2001). After the initial stage of spin up the fully coupled version of RASM with bio-geochemical (BGC) components was run for three years starting at the first of September 1979. This three-year period was repeated three times in order to avoid the initial shock of any component, especially the ocean and sea-ice BGC parts. The RASM production simulation, the results of which are analyzed in this paper, was started in September 1979 and continued through the end of 2018. The lateral boundary conditions at North Atlantic and Pacific sides utilized temperature and salinity information (PHC 3.0) with 30-day restoring strength. The upper and lateral atmospheric boundary conditions for the atmospheric model were based on ERA-Interim reanalysis (Dee & Coauthors, 2011).

## 2.2 Marine biogeochemical model

The ocean BGC component in RASM is a medium-complexity Nutrients-Phytoplankton-Zooplankton-Detritus (NPZD) model (Moore, Doney, Kleypas, Glover, & Fung, 2002; Moore, Doney, & Lindsay, 2004; Moore, Lindsay, Doney, Long, & Misumi, 2013). The model has three phytoplankton categories: diatoms, small phytoplankton and diazotrophs, with explicit carbon, iron (Fe) and chlorophyll-*a* (chl-*a*) pools for each category, as well as an explicit Si pool for diatoms and an implicit  $\text{CaCO}_3$  pool for small phytoplankton. Other state variables are:  $\text{NO}_3$ ,  $\text{NH}_4$ , Fe, Si,  $\text{PO}_4$ , a herbivorous phytoplankton pool, dissolved organic nitrogen, carbon, iron and phosphate (DON, DOC, DOfe, and DOP), oxygen, dissolved inorganic carbon (DIC) and alkalinity.

169 The column package version of CICE includes two BGC parameterizations. One  
 170 is a skeletal layer (SKL) parameterization in which all biological processes are assumed  
 171 to be confined to a 3-cm layer at the bottom of the ice. The other is a vertical (ZBGC)  
 172 parameterization in which biological activity is distributed throughout the ice column.  
 173 In this study, we use the ZBGC parameterization for all our simulations. The model in-  
 174 cludes three algal categories (diatoms, small phytoplankton and *Phaeocystis sp*), two dis-  
 175 solved organic carbon tracers (polysaccharids and lipids), a dissolved organic nitrogen  
 176 tracer,  $\text{NO}_3$ ,  $\text{NH}_4$ ,  $\text{SiO}_3$ , dissolved Fe (FeD), dimethylsulfide (DMS), and dissolved and  
 177 particulate dimethylsulfoniopropionate (DMSPd and DMSPp). Additional details on  
 178 the sea ice BGC component can be found in Jeffery et al. (2020).

### 179 3 Conditions required for under-ice blooms

#### 180 3.1 Nutrient requirements

181 Here we focus on nitrate as the limiting nutrient for under-ice blooms. A bloom  
 182 occurs when phytoplankton growth rate exceeds the loss rate. If we assume that phy-  
 183 toplankton cell carbon to nitrogen ratios are fixed, then algal growth rate ( $G_{\text{NO}_3}$ ) and  
 184 loss rate ( $L_{\text{NO}_3}$ ) are determined by nitrate uptake, and bloom permitting conditions  
 185 occur when

$$L_{\text{NO}_3} = G_{\text{NO}_3} = \mu_{max} \left( \frac{\text{NO}_3}{\text{NO}_3 + \kappa_{\text{NO}_3}} \right), \quad (1)$$

186 where  $\mu_{max}$  is the maximum algal growth rate, and  $\kappa_{\text{NO}_3}=2.5 \text{ mmol/m}^3$  is the half-saturation  
 187 constant for nitrate uptake. The critical value of nitrate concentration necessary to pro-  
 188 duce a bloom can then be calculated as

$$\text{NO}_3 = \frac{L_{\text{NO}_3} \times \kappa_{\text{NO}_3}}{\mu_{max} \left( 1 - \frac{L_{\text{NO}_3}}{\mu_{max}} \right)}. \quad (2)$$

189  $L_{\text{NO}_3}$  and  $\mu_{max}$  are both temperature-dependent quantities, with the temperature  
 190 dependence being defined in RASM as  $T_{dep} = 2.0^{((T+273.16)-(30.0+273.16))/10.0}$ . Because  
 191 our analysis focuses on chl-*a* in the surface layer,  $T$  is assumed to be  $-1.8^\circ \text{C}$  as a rep-  
 192 resentative surface water temperature under the ice. Thus,  $\mu_{max}$  can be defined as  $\text{PC}_{ref} T_{dep}$ ,  
 193 where  $\text{PC}_{ref}=4.8 \text{ days}^{-1}$  is the maximum diatom growth rate at  $T_{ref}=30^\circ \text{C}$  and  $L_{\text{NO}_3}$   
 194  $= \text{mort} \times T_{dep}$ , where  $\text{mort}=0.15 \text{ day}^{-1}$  is the diatom mortality rate. Given these assump-  
 195 tions, the critical nitrate concentration required to permit a bloom is  $\text{NO}_3=0.08 \text{ mmol/m}^3$ .

#### 196 3.2 Light requirements

197 When sufficient nutrients are available, the PAR becomes the limiting factor for  
 198 under-ice blooms. In their model study based on the Sverdrup critical depth hypothe-  
 199 sis (Sverdrup, 1953), Horvat et al. (2017) related PAR beneath the ice to melt ponds con-  
 200 centration, computing a critical melt pond fraction that would be necessary for an under-  
 201 ice bloom to occur. Here we adopt a number of Horvat et al.'s assumptions, as well as  
 202 their use of Sverdrup's hypothesis, to estimate the critical PAR levels necessary for an  
 203 under-ice bloom. While RASM does not include PAR among its variables, it does include  
 204 shortwave radiation through the ice to the ocean surface. We therefore use the 0.43 PAR  
 205 to shortwave ratio estimated by Olofsson, Van Laake, and Eklundh (2007) to determine  
 206  $I_0$ , or PAR at the ocean surface under the ice. PAR at depth  $z$  can then be computed  
 207 as

$$I(z) = I_0 e^{\kappa_w z}, \quad (3)$$

208 where  $\kappa_w = 1.2 \text{ m}^{-1}$  is the bulk irradiance coefficient of PAR in clear water (Pegau, 2002).

209 Following Horvat et al. (2017), we assume a constant, depth-independent phyto-  
 210 plankton decay rate  $\Gamma$  ( $\text{m}^{-1}\text{s}^{-1}$ ) throughout the mixed layer. We then determine the phyto-  
 211 plankton growth rate as

$$G(D) = \frac{M}{D} \int_{-D}^0 I(z) dz \quad (4)$$

212 where  $D$  is the mixed layer depth, and  $M$  is a coefficient relating phytoplankton growth  
 213 rate to PAR availability, so that  $\Gamma/M$  is the compensation irradiance. For our calcula-  
 214 tions, we used the Eastern Arctic compensation irradiance estimates of Regaudie-de-Gioux  
 215 and Duarte (2010) and set  $\Gamma/M = 1.3 \text{ mol quanta m}^{-2} \text{ day}^{-1}$ , which was multiplied by  
 216 a conversion factor for PAR from sunlight of  $2.5 \text{ W mol}^{-1} \text{ day}^{-1}$  to give us  $\Gamma/M = 3.25$   
 217  $\text{W m}^{-2}$ .

218 As discussed in the section above, bloom conditions require that the phytoplank-  
 219 ton growth rate exceeds the loss rate. We can therefore determine the critical value for  
 220  $I_0$  by setting  $G(D) = \Gamma$  and solving for  $I_0$  to get

$$I_0 = D\kappa_w \frac{\Gamma}{M} (1 - e^{-\kappa_w D})^{-1}. \quad (5)$$

## 221 4 Model results

222 Under sea-ice blooms in the Arctic are composed primarily of diatoms, both in ob-  
 223 servations (Arrigo et al., 2014) and in RASM. We therefore focus on diatoms in our eval-  
 224 uation of model results. All references to chl-*a* concentration and primary production  
 225 in this paper refer specifically to diatom values. Figure 2 (a) shows modeled surface chl-  
 226 *a* distribution in the northern Chukchi Sea during July 3-8 2011, corresponding to the  
 227 dates when an under-ice bloom was detected in the region during the 2011 ICESCAPE  
 228 survey (Arrigo et al. 2012). While a bloom is present in the model in the north-west cor-  
 229 ner of the region, it is located further north than the observed bloom, and the modeled  
 230 chl-*a* concentrations are lower than the observed concentrations. Modeled ice concen-  
 231 trations for this time period (shown as red contours in Figure 2) indicate that the mod-  
 232 eled sea ice has retreated further north compared to the satellite-observed sea ice con-  
 233 ditions, and surface nitrate concentrations (not shown) are near zero throughout the re-  
 234 gion, suggesting that the model bloom has peaked earlier in the season and has consumed  
 235 most available nutrients. The chl-*a* distribution for Jun 20-24 2011 (Figure 2 (b)), when  
 236 modeled sea ice extent was similar to observed extent during the ICESCAPE cruise, shows  
 237 improved correspondence to the observed bloom, with the location and spatial extent  
 238 of the modeled bloom being similar to observations. However, while the maximum mod-  
 239 eled chl-*a* value for the region is  $21.45 \text{ mg/m}^3$ , the observed values reach as high as  $64.7$   
 240  $\text{mg/m}^3$ . Point-to-point comparison of modeled versus observed chl-*a* values is shown in  
 241 Figure 3. The discrepancy between maximum modeled and observed values might be due  
 242 to several reasons. One is the fact that that model surface atmospheric conditions, such  
 243 as winds, clouds, radiative fluxes which force sea ice, are not prescribed from a reanal-  
 244 ysis but ‘predicted’ from an active atmospheric model in the fully coupled configuration  
 245 of RASM. Another possible reason could be the fact that the ocean model’s horizontal  
 246 resolution, while eddy-permitting, is not eddy-resolving and likely doesn’t fully capture  
 247 the mesoscale ocean dynamics, hence also small-scale local chl-*a* gradients that are seen  
 248 in the observations. Additional discrepancies in the modeled sea ice cover might be re-  
 249 lated to inadequate coupling of horizontal momentum transfer across the atmosphere -  
 250 sea ice - ocean interface.

251 When considering model results over a larger region of the western Arctic (Figure  
 252 4), it is clear that that the full extent of the 2011 under sea-ice bloom in the western Arc-  
 253 tic was significantly larger than the area covered by the ICESCAPE observations. This

254 bloom appears annually throughout the simulation period, indicating that under-ice blooms  
 255 are not a recent phenomenon. At the same time model results reveal relatively signif-  
 256 icant variability in the under sea-ice bloom distribution, magnitude and timing. To demon-  
 257 strate this, Figures 4, 6 and 8 are shown with the modeled surface chl-*a* distributions  
 258 for the western Arctic bloom (WB) region, designated as the region between latitudes  
 259 70° N and 78° N and longitudes 150° E to 150° W, for the years 2011, 2001 and 1991.

260 In addition to the western Arctic bloom region described above, a second bloom  
 261 of similar duration but of lower chl-*a* is simulated by the model in the eastern Arctic,  
 262 and it also varies in distribution, magnitude and timing. Figures 5, 7 and 9 show the  
 263 surface chl-*a* distributions within the eastern Arctic bloom (EB), designated as the re-  
 264 gion between latitudes 75° N and 85° N and longitudes 0° to 90° E, for the same years  
 265 2011, 2001 and 1991 as in the case of and for comparison with the WB results.

## 266 5 Discussion

267 To summarize the above results, the left side of Figure 10 shows the time series  
 268 of spatially-integrated surface chl-*a* for both the EB and WB regions during May, June  
 269 and July of 1991, 2001 and 2011. Previous satellite observations suggest that Arctic spring  
 270 phytoplankton blooms are beginning to occur earlier in the year due to earlier sea-ice  
 271 breakup and decreasing sea-ice concentrations in early summer (Kahru, Brotas, Manzano-  
 272 Sarabia, & Mitchell, 2011). Our results show a similar pattern for the eastern bloom,  
 273 which reached peak chl-*a* levels during June 19-23 in 1991, June 12-16 in 2001, and June  
 274 7-11 in 2011. However, the western bloom does not show the same pattern, with the 2001  
 275 peak (June 27-July 1) occurring later than the 1991 peak (June 22-26).

276 For both regions, the post-peak decline of total under sea-ice chl-*a* is affected by  
 277 decreasing sea-ice coverage as well as by phytoplankton mortality. The EB region shows  
 278 similar coverage for all three years of our analysis, with approximately 50% of the re-  
 279 gion still being covered by sea-ice by the end of July. In particular, 2001 and 2011 both  
 280 show EB chl-*a* total decreasing from mid-June through July at a faster rate than the sea-  
 281 ice coverage, indicating that the decrease is due primarily to phytoplankton loss. This  
 282 loss cannot be explained by nutrient depletion, as is discussed below. By contrast, the  
 283 rate of total chl-*a* decrease in the WB region corresponds more closely to the rate of sea-  
 284 ice decrease, particularly in 2011, when under sea-ice chl-*a* declines to near zero at the  
 285 same rate that the region becomes ice-free, suggesting that little to no actual phytoplank-  
 286 ton loss is taking place. This is further supported by the dashed lines in the top panel  
 287 of Figure 11, which show the PP for the entire WB remaining relatively constant after  
 288 the under sea-ice bloom peaks.

289 Rows 2-4 in Figures 4 to 9 show the PAR (row 2) nutrient (row 3) and combined  
 290 nutrient and PAR (row 4) conditions for the western and eastern under-ice blooms. For  
 291 both regions, the period of May 15-19 in all years has been designated as "pre-bloom,"  
 292 while the period of July 21-25 was designated as "post-bloom." Red areas in the figures  
 293 indicate the regions where nutrient and light conditions meet the critical requirements  
 294 for bloom formation, as discussed in sections 3.1 and 3.2. During the pre-bloom period,  
 295 nitrate concentrations are above the critical threshold throughout the ice-covered Arctic,  
 296 reflecting the build-up of nutrients during the winter. As the blooms progress, nutri-  
 297 ent concentrations become reduced, with the greater decrease occurring in the west-  
 298 ern bloom region; the eastern and central Arctic remain nutrient-replete even into the  
 299 post-bloom period. Therefore, the beginning of the under sea-ice blooms is triggered by  
 300 PAR availability, after which the blooms persist until the available nutrients are depleted  
 301 or until the region becomes ice-free (at which point the bloom is no longer considered  
 302 an under sea-ice bloom). The critical PAR criteria of Equation 5 can thus allow us to  
 303 distinguish between true under-ice blooms and blooms that originally formed in open  
 304 water and were subsequently advected beneath the ice. The majority of EB area in RASM

305 does not meet the critical PAR criteria in 2011 or 1991. However, the entire EB region  
 306 still has a bloom in all three years of our study, suggesting an advective origin. This con-  
 307 clusion is consistent with the study of Johnsen et al. (2018), in which an under-ice bloom  
 308 was observed in May 2010 northwest of Svalbard in our EB region and attributed to ad-  
 309 vection, with northward flowing water masses and southward flowing sea ice.

310 The advective origin of the EB is further supported by the differences in the chl-  
 311 *a* and PP time series for the two blooms. The April chl-*a* totals integrated over the top  
 312 150 m for the WB (Figure 10 (a)) are near zero for all years shown. In 2011, the chl-*a*  
 313 totals drop to zero again by August, while in 2001 and 1991 the totals drop below  $5 \times 10^7$   
 314 kg but remain non-zero. This is consistent with the PP time series for the region (Fig-  
 315 ure 11 (a)), which begins near zero in April for all years and decreases to zero again in  
 316 August for 2011 but not for the other two years. In contrast, the EB chl-*a* totals for all  
 317 three years begin at approximately  $1.5 \times 10^7$  kg in April and do not drop below  $2 \times 10^7$   
 318 kg throughout the time series. Likewise, the PP for the EB remains non-zero for the en-  
 319 tire time span shown in Figure 11. In fact, the full-year PP time series for the EB (not  
 320 shown) indicates positive PP totals in the top 150 m starting in mid-February. The EB  
 321 region does not have sufficient light to support photosynthesis that early in the year, in-  
 322 dicating that the chl-*a* and PP totals must be the result of a bloom advected from an  
 323 ice-free location farther south. While the maximum PP totals for the EB region are ap-  
 324 proximately half of the WB totals, the early start and long duration of the EB still make  
 325 it a significant factor in the total PP for the Arctic region.

326 RASM simulations indicate that favorable PAR conditions for under-ice blooms have  
 327 existed in the western Arctic at least as far back as 1991, allowing massive blooms to oc-  
 328 cur annually on the shelf and along the shelf break in that region. Satellite-derived es-  
 329 timates of sea-ice thickness have indicated that Arctic sea ice has been growing thinner  
 330 since at least 1982, as multi-year ice is replaced by first-year ice (Maslanik et al., 2007).  
 331 In addition, the presence and extent of melt ponds on the surface of the sea ice in the  
 332 Western Arctic has been increasing over the last few decades (Hutchings & Faber, 2018).  
 333 The model results suggest that if these trends continue, PAR penetration through sea-  
 334 ice to the ocean surface will increase, leading to larger and earlier-occurring under sea-  
 335 ice blooms, with a corresponding increase in Arctic primary production and nutrient con-  
 336 sumption. *In situ* sampling in the EB and WB regions in the next few years would serve  
 337 to confirm these results and provide a clearer picture of the effects of sea-ice reduction  
 338 on Arctic Ocean biogeochemistry.

## 339 Figure Captions

340 Figure 1: The atmosphere/land and ice/ocean domains of the Regional Arctic System  
 341 Model

342 Figure 2: Modeled surface chl-*a* distribution in the northern Chukchi Sea during July  
 343 3-8 2011 (a) and Jun 20-24 2011 (b). Circles represent the locations and observed sur-  
 344 face chl-*a* concentrations for hydrographic stations sampled during the July 2011 ICESCAPE  
 345 cruise (Arrigo et al., 2012). Red lines indicate modeled ice concentration; green lines in  
 346 both panels indicate observed ice concentration from satellite during the ICESCAPE cruise.

347 Figure 3: Surface chl-*a* distributions for the hydrographic stations shown in Figure 2 and  
 348 for the corresponding model grid cells.

349 Figure 4: Top row shows the modeled ocean surface chl-*a* distributions before, at peak  
 350 chl-*a*, and after the Western Arctic Bloom during 2011 in the region where ice fraction  
 351 is greater than 50%. Red areas in the second row indicate the regions where PAR through  
 352 the ice to the ocean surface exceeds the critical value as determined in Section 3.2. Red  
 353 areas in the third row indicate the regions where surface nitrate concentration exceeds  
 354 the critical value as determined in Section 3.1. Red areas in the bottom row indicate the

355 regions where both PAR and nitrate exceed their critical values. Pink contour in-  
 356 dicates the region of the 2011 ICESCAPE cruise (Arrigo et al., 2012)

357 Figure 5: Same as in Figure 5, but for the Eastern Arctic Bloom.

358 Figure 6: Same as in Figure 5, but for the Western Arctic Bloom in 2001.

359 Figure 7: Same as in Figure 5, but for the Eastern Arctic Bloom in 2001.

360 Figure 8: Same as in Figure 5, but for the Western Arctic Bloom in 1991.

361 Figure 9: Same as in Figure 5, but for the Eastern Arctic Bloom in 1991.

362 Figure 10: Time series of spatially integrated surface chl-*a* (green lines) and percentage  
 363 sea-ice area (black lines) for the eastern and western under sea-ice bloom areas for the  
 364 years 1991, 2001 and 2001. Vertical green bars delineate the 5-day period surrounding  
 365 the date of the chl-*a* maximum for each time series. Vertical gray bars delineate July 3-  
 366 8 2011. Dashed lines indicate the pre-bloom and post-bloom periods as shown in the first  
 367 and last columns of Figures 4-9

368 Figure 11: Spatially-integrated model primary production for the WB and EB regions  
 369 for May, June and July of 1991, 2001 and 2001. Dashed lines represent primary produc-  
 370 tion for the entire region. Solid lines represent primary production for the portion of the  
 371 region where ice concentration is greater than 50%.

## 402 Acknowledgments

403 We acknowledge Kevin Arrigo for providing the observational data from the summer 2011  
 404 ICESCAPE cruise. We also acknowledge Andrew Roberts for the creation of Figure 1.  
 405 This research was partially supported by the following: Collaborative Research: Under-  
 406 standing Arctic Marine Biogeochemical Response to Climate Change for Seasonal to Decadal  
 407 Prediction Using Regional and Global Climate Models, Award number IAA1417888, Pro-  
 408 gram NSF ARCSS; High-Latitude Application and Testing of Earth System Models -  
 409 Phase II, Award number IAA89243019SSC000030, Program DOERGMA; Ministry of  
 410 Science and Higher Education in Poland in the frame of co-financed international project  
 411 agreement Award number 3808/FAO/2017/0 RASMer. Computational resources have  
 412 been provided by the DOD High Performance Computing Modernization Program. The  
 413 authors declare no competing interests. **Data and materials availability:** RASM model  
 414 output is archived at the U. S. DoD HPCMP, which requires security clearance to ac-  
 415 cess but can be made available upon request. The RASM model code is archived on the  
 416 subversion server at the Naval Postgraduate School (<https://svn.nps.edu>) and cannot  
 417 be publicly available due to copyright restriction at this time. Access may be granted  
 418 by contacting Wieslaw Maslowski ([maslowski@nps.edu](mailto:maslowski@nps.edu)).

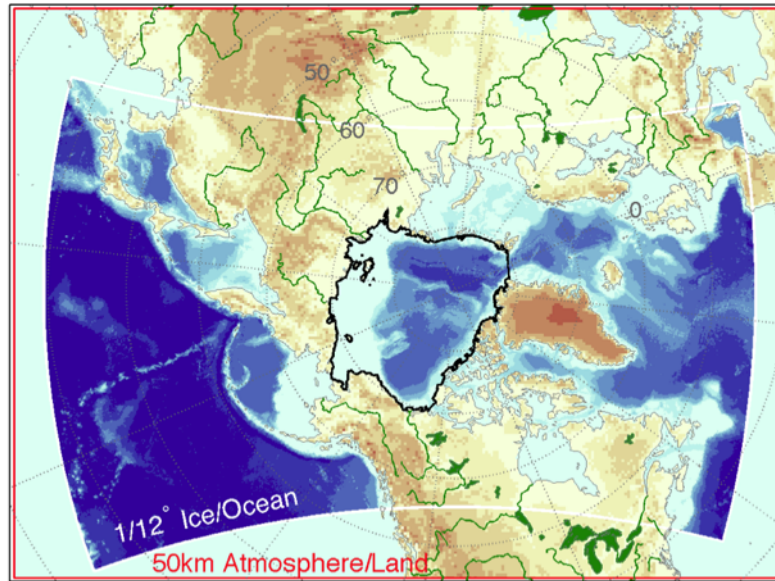
## 419 References

- 420 Arrigo, K. R., Perovich, D. K., Pickart, R. S., Brown, Z. W., van Dijken, G. L.,  
 421 Lowry, K. E., ... Swift, J. H. (2012). Massive phytoplankton blooms under  
 422 Arctic sea ice. *Science*, *336*, 1408.
- 423 Arrigo, K. R., Perovich, D. K., Pickart, R. S., Brown, Z. W., van Dijken, G. L.,  
 424 Lowry, K. E., ... Swift, J. H. (2014). Phytoplankton blooms beneath the sea  
 425 ice in the Chukchi sea. *Deep-Sea Res. II*, *105*, 1-16.
- 426 Brunke, M. A., Cassano, J. J., Dawson, N., DuVivier, Gutowski, W. J., Hamman,  
 427 J., ... Zeng, X. (2018). Evaluation of the atmosphere-land-ocean-sea ice in-  
 428 terface processes in the Regional Arctic System Model version 1 (RASM1)  
 429 using local and globally gridded observations. *Geosci. Model. Dev.*, *11*,  
 430 4817-4841. doi: 10.5194/gmd-11-4817-2018
- 431 Cassano, J., DuVivier, A., Roberts, A., Hughes, M., Seefeldt, M., Brunke, M., ...

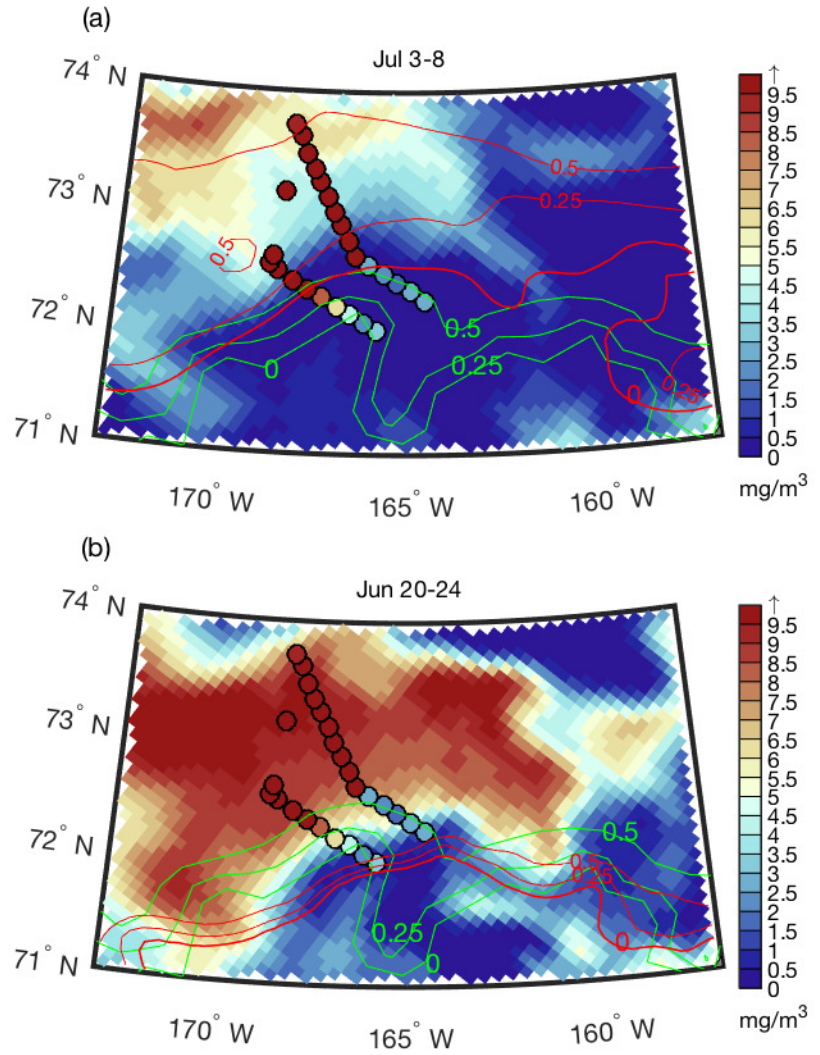
- 432 Zeng, X. (2017). Development of the Regional Arctic System Model (RASM):  
 433 Near-surface atmospheric climate sensitivity. *J. Climate*, *30*, 5729-5753. doi:  
 434 10.1175/JCLI-D-15-0775.1
- 435 Dee, D. P., & Coauthors. (2011). The ERA-Interim reanalysis: configuration and  
 436 performance of the data assimilation system. *Q.J.R. Meteorol. Soc.*, *137*, 553-  
 437 597. doi: 10.1002/qj.828
- 438 DuVivier, A. K., Cassano, J. J., Craig, A., Hamman, J., Maslowski, W., Nijssen, B.,  
 439 ... Roberts, A. (2016). Winter Atmospheric Buoyancy Forcing and Oceanic  
 440 Response during Strong Wind Events around Southeastern Greenland in the  
 441 Regional Arctic System Model (RASM) for 1990–2010. *J. Climate*, *29*, 975-  
 442 994. doi: 10.1175/JCLI-D-15-0592.1
- 443 Fortier, M., Fortier, L., Michel, C., & Legendre, L. (2002). Climatic and biological  
 444 forcing of the vertical flux of biogenic particles under seasonal Arctic sea ice.  
 445 *Mar. Ecol. Prog. Ser.*, *225*, 1-16.
- 446 Fukuchi, M., Watanabe, K., Tanimura, A., Hoshiai, T., Sasaki, H., Satoh, H., &  
 447 Yamagushi, Y. (1989). A phytoplankton bloom under sea ice recorded with a  
 448 moored system in Lagoon Saroma Ko, Hokkaido, Japan. *Proc. Natl. Inst. Polar*  
 449 *Res. (NIPR) Symp. Polar Biol.*, *2*, 9-15.
- 450 Grebmeier, J., & Barry, J. P. (1991). The influence of oceanographic processes on  
 451 pelagic-benthic coupling in polar regions: a benthic perspective. *J. Mar. Syst.*,  
 452 *2*, 495-518.
- 453 Grebmeier, J., Cooper, L. W., Feder, H. M., & Sirenko, B. I. (2006). Ecosystem  
 454 dynamics of the Pacific-influenced Northern Bering and Chukchi Seas in the  
 455 Amerasian Arctic. *Prog. Oceanogr.*, *71*, 331-361.
- 456 Hamman, J., Nijssen, B., Roberts, A., Craig, A., Maslowski, W., & Osinski, R.  
 457 (2017). The coastal streamflow flux in the Regional Arctic System Model. *J.*  
 458 *Geophys. Res.-Oceans*, *122*, 1683–1701. doi: 10.1002/2016JC012323
- 459 Hill, V. J., Light, B., Steele, M., & Zimmerman, R. (2018). Light availabil-  
 460 ity and phytoplankton growth beneath Arctic sea ice: Integrating obser-  
 461 vations and modeling. *J. Geophys. Res.-Oceans*, *123*, 3651-3667. doi:  
 462 10.1029/2017JC013617
- 463 Horvat, C., Jones, D. R., Iams, S., Schroeder, D., Flocco, D., & Feltham, D. (2017).  
 464 The frequency and extent of sub-ice phytoplankton blooms in the Arctic  
 465 Ocean. *Sci. Adv.*, *3*. doi: 10.1126/sciadv.1601191
- 466 Hunke, E. C., Lipscomb, W. H., Turner, A. K., Jeffery, N., & Elliot, S. (2015).  
 467 CICE: The Los Alamos sea ice model. documentation and software user's  
 468 manual version 5.1 (la-cc-06-12).
- 469 Hunke, E. C., Lipscomb, W. H., Turner, A. K., Jeffery, N., & Elliot, S. (2016).  
 470 CICE: The Los Alamos sea ice model. documentation and software user's  
 471 manual zbgc\_colpkg modifications to version 5.
- 472 Hutchings, J., & Faber, M. K. (2018). Sea-Ice Morphology Change in the  
 473 Canada Basin Summer: 2006–2015 Ship Observations Compared to Ob-  
 474 servations From the 1960s to the Early 1990s. *Front. Earth Sci.*. doi:  
 475 <https://doi.org/10.3389/feart.2018.00123>
- 476 Jeffery, N., Maltrud, M. E., Hunke, E. C., Wang, S., Wolf, J., Turner, A. K., ...  
 477 Calvin, K. (2020). Investigating controls on sea ice algal production using  
 478 E3SMv1.1-BGC. *Ann. Glaciol.*, *1-22*. doi: 10.1017/aog.2020.7
- 479 Jin, M., Deal, C., Lee, S. H., Elliott, S., Hunke, E., Maltrud, M., & Jeffery, N.  
 480 (2012). Investigation of Arctic sea ice and ocean primary production for  
 481 the period 1992-2007 using a 3-D global ice-ocean ecosystem model. *Deep-Sea*  
 482 *Res. II*, 28-35.
- 483 Jin, M., Deal, C., Maslowski, W., Matrai, P., Roberts, A., Osinski, R., ... Wang, S.  
 484 (2018). Effects of model resolution and ocean mixing on forced ice-ocean physi-  
 485 cal and biogeochemical simulations using global and regional system models. *J.*  
 486 *Geophys. Res.-Oceans*, *122*. doi: 10.1002/2017JCO13365

- 487 Jin, M., Hutchins, J., Kawaguchi, Y., & Kikuchi, T. (2012). Ocean mixing with lead-  
488 dependent subgrid scale brine rejection parameterization in climate model. *J.*  
489 *Ocean U. China*, *11*, 473-480.
- 490 Johnsen, M., G. Norli, Moline, M., Robbins, I., von Quillfeldt, C., Sorensen, K., Cot-  
491 tier, F., & Berge, J. (2018). The advective origin of an under-ice spring bloom  
492 in the Arctic Ocean using multiple observational platforms. *Polar Biol.*, *41*,  
493 1197-1216. doi: 10.1007/s00300-018-2278-5
- 494 Kahru, M., Brotas, V., Manzano-Sarabia, M., & Mitchell, B. G. (2011). Are phy-  
495 toplankton blooms occurring earlier in the arctic? *Glob. Change Biol.*. doi: 10  
496 .1111/j.1365-2486.2010.02312.x
- 497 Large, W. G., & Yeager, S. G. (2009). The global climatology of an interannually  
498 varying air-sea flux data set. *Clim. Dyn.*, *33*, 341-364.
- 499 Legendre, L., Ingram, R. G., & Poulin, M. (1989). Physical control of phytoplank-  
500 ton production under sea ice (Manitounuk Sound, Hudson Bay). *Can. J. Fish.*  
501 *Aquat. Sci.*, *38*, 1385-1392.
- 502 Lowry, K. E., van Dijken, G., & Arrigo, K. R. (2014). Evidence of under-ice phyto-  
503 plankton blooms in the Chukchi Sea from 1998 to 2012. *Deep-Sea Res. II*, *105*,  
504 105-117.
- 505 Manizza, M., Le Quere, C., Watson, A. J., & Buitenhuis, E. T. (2005). Bio-optical  
506 feedbacks among phytoplankton, upper ocean physics and sea-ice in a global  
507 model. *Geophys. Res. Lett.*, *32*. doi: 10.1029/2004GL020778
- 508 Maslanik, J. A., Fowler, C., Stroeve, J., Drobot, S., Zwally, J., Yi, D., & Emery,  
509 W. (2007). A younger, thinner Arctic ice cover: Increased potential for rapid,  
510 extensive sea-ice loss. *Geophys. Res. Lett.*, *34*. doi: 10.1029/2007GL032043
- 511 Moore, J. K., Doney, S. C., Kleypas, J. C., Glover, D. M., & Fung, I. Y. (2002). An  
512 intermediate complexity marine ecosystem model for the global domain. *Deep-*  
513 *Sea Res. II*, *49*, 403-462.
- 514 Moore, J. K., Doney, S. C., & Lindsay, K. (2004). Upper ocean ecosystem dynamics  
515 and iron cycling in a global three-dimensional model. *Global Biogeochem. Cy.*,  
516 *18*. doi: 10.1029/2004GB002220
- 517 Moore, J. K., Lindsay, K., Doney, S. C., Long, M. C., & Misumi, K. (2013). Marine  
518 ecosystem dynamics and biological cycling in the Community Earth System  
519 Model (CESM) [CESM1(BGC)]: Comparison of the 1990s with the 2090s  
520 under the RCP4.5 and RCP8.5 scenarios. *J Climate*, *26*, 9291-9312.
- 521 Olofsson, P., Van Laake, P. E., & Eklundh, L. (2007). Estimation of absorbed par  
522 across scandinavia from satellite measurements: Part i: Incident par. *Remote*  
523 *Sens Environ*, *110*, 252-261.
- 524 Pegau, W. S. (2002). Inherent optical properties of the central Arctic surface waters.  
525 *J. Geophys. Res.*, *107*.
- 526 Regaudie-de-Gioux, A., & Duarte, C. M. (2010). Compensation irradiance for plank-  
527 tonic community metabolism in the ocean. *Global Biogeochem Cy*, *24*. doi: 10  
528 .1029/2009GB003639
- 529 Roberts, A., Craig, A., Maslowski, W., Osinski, R., Duvivier, A., Hughes, M., ...  
530 Brunke, M. (2015). Simulating transient ice-ocean Ekman transport in the  
531 Regional Arctic System Model and Community Earth System Model. *Ann.*  
532 *Glaciol.*, *56*, 211-228. doi: 10.3189/2015AoG69A760
- 533 Roberts, A., Hunke, E. C., Allard, R., Bailey, D. A., Craig, A. P., Lemieux, J. F.,  
534 & Turner, M. D. (2018). Quality control for community-based sea-ice model  
535 development. *Philos. T. R. Soc. A*, *376*, 1-18. doi: 10.1098/rsta.2017.0344
- 536 Sigler, M. F., Renner, M., Danielson, S. L., Eisner, L. B., Lauth, R. R., Kuletz,  
537 K. J., ... Hunt, G. L. (2011). Fluxes, fins and feathers: relationships among  
538 the Bering, Chukchi and Beaufort Seas in a time of climate change. *Oceanogr.*,  
539 *24*, 251-265.
- 540 Steele, M., Morley, R., & Ermold, W. (2001). PHC: A global ocean hydrography  
541 with a high quality Arctic Ocean. *J. Climate*, *14*, 2079-2087.

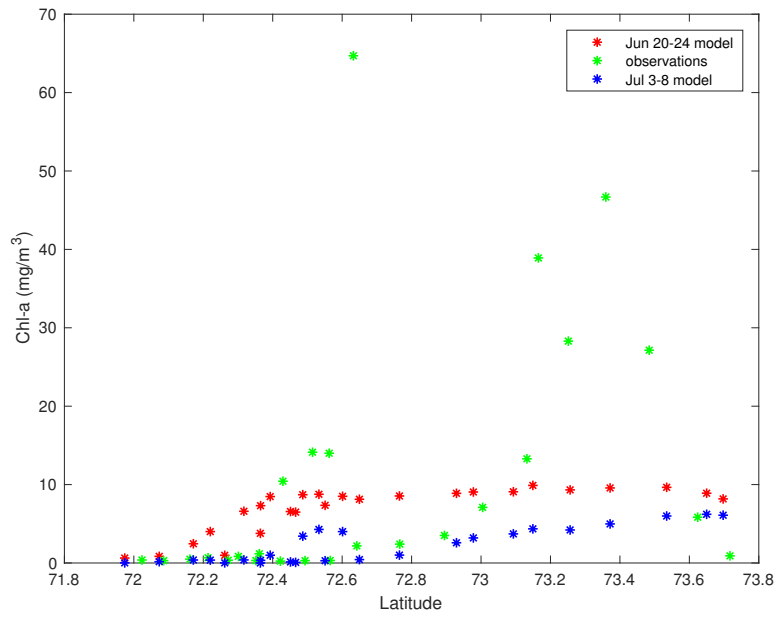
- 542 Sverdrup, H. U. (1953). On conditions for the vernal blooming of phytoplankton. *J.*  
543 *Cons. Perm. Int. Explor. Mer.*, *18*, 287-295.
- 544 Turner, A. K., & Hunke, E. C. (2015). Impacts of a mushy-layer thermodynamic ap-  
545 proach in global sea-ice simulations using the CICE sea-ice model. *J. Geophys.*  
546 *Res.-Oceans*, *120*, 1253-1275.
- 547 Wilchinsky, A. V., & Feltham, D. L. . (2004). A continuum anisotropic model of sea  
548 ice dynamics. *P. R. Soc. London*, *460*, 2105-2140.
- 549 Zhang, J., Ashjian, C., Campbell, R., Spitz, Y. H., Steele, M., & Hill, V. (2015).  
550 The influence of sea ice and snow cover and nutrient availability on the forma-  
551 tion of massive under-ice phytoplankton blooms in the Chukchi Sea. *Deep-Sea*  
552 *Res. II*, *118*, 122-135.



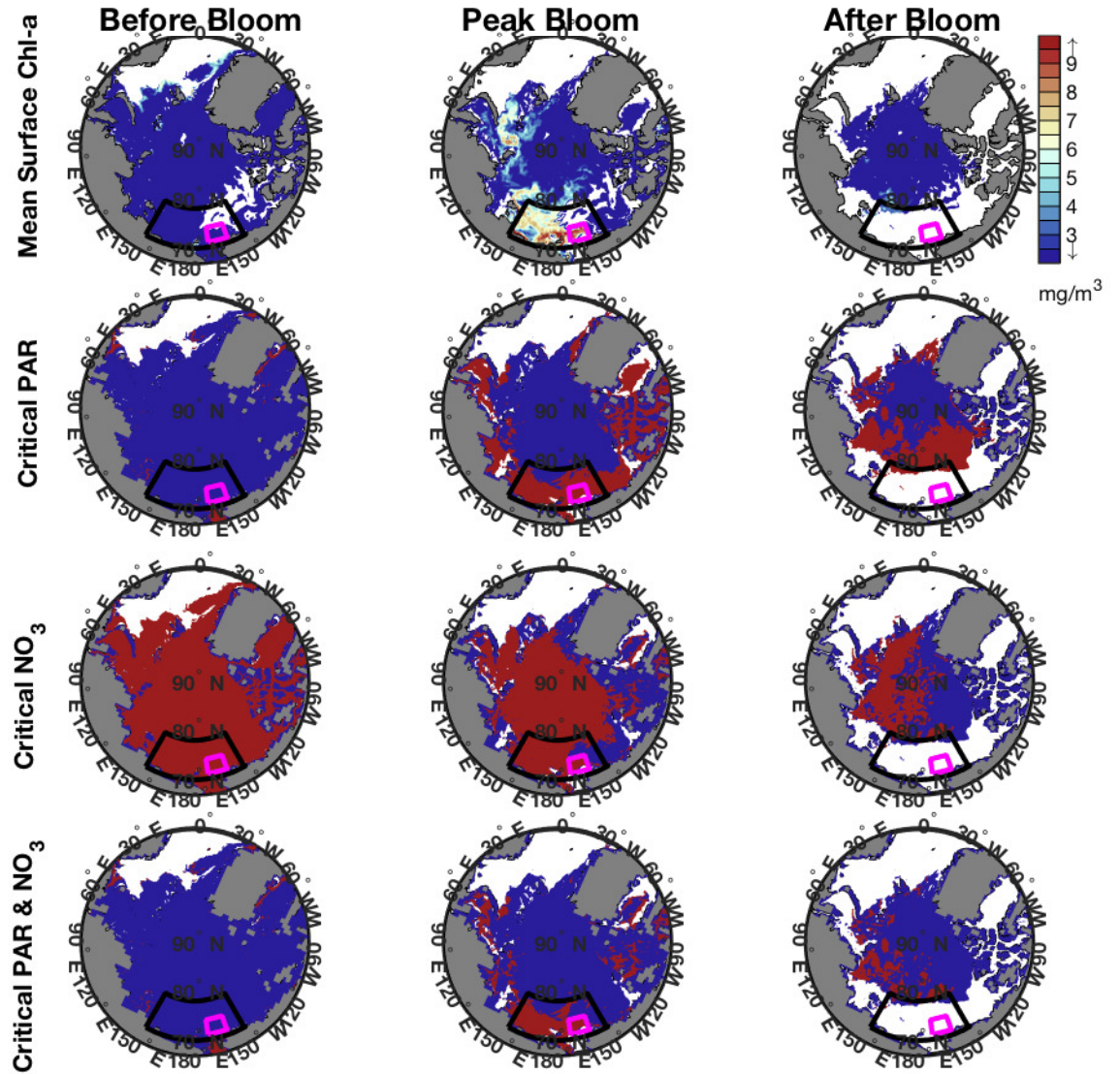
372 **Figure 1.** The atmosphere/land and ice/ocean domains of the Regional Arctic System Model



373 **Figure 2.** Modeled surface chl-*a* distribution in the northern Chukchi Sea during July 3-8  
 374 2011 (a) and Jun 20-24 2011 (b). Circles represent the locations and observed surface chl-*a*  
 375 concentrations for hydrographic stations sampled during the July 2011 ICESCAPE cruise (Arrigo  
 376 et al., 2012). Red lines indicate modeled ice concentration; green lines in both panels indicate  
 377 observed ice concentration from satellite during the ICESCAPE cruise.



378 **Figure 3.** Surface chl-*a* distributions for the hydrographic stations shown in Figure 2 and for  
 379 the corresponding model grid cells.



380 **Figure 4.** Top row shows the modeled ocean surface chl-*a* distributions before, at peak chl-*a*,  
 381 and after the Western Arctic Bloom during 2011 in the region where ice fraction is greater than  
 382 50%. Red areas in the second row indicate the regions where PAR through the ice to the ocean  
 383 surface exceeds the critical value as determined in Section 3.2. Red areas in the third row in-  
 384 dicate the regions where surface nitrate concentration exceeds the critical value as determined  
 385 in Section 3.1. Red areas in the bottom row indicate the regions where both PAR and nitrate  
 386 exceed their critical values. Pink contour indicates the region of the 2011 ICESCAPE cruise  
 387 (Arrigo et al., 2012)

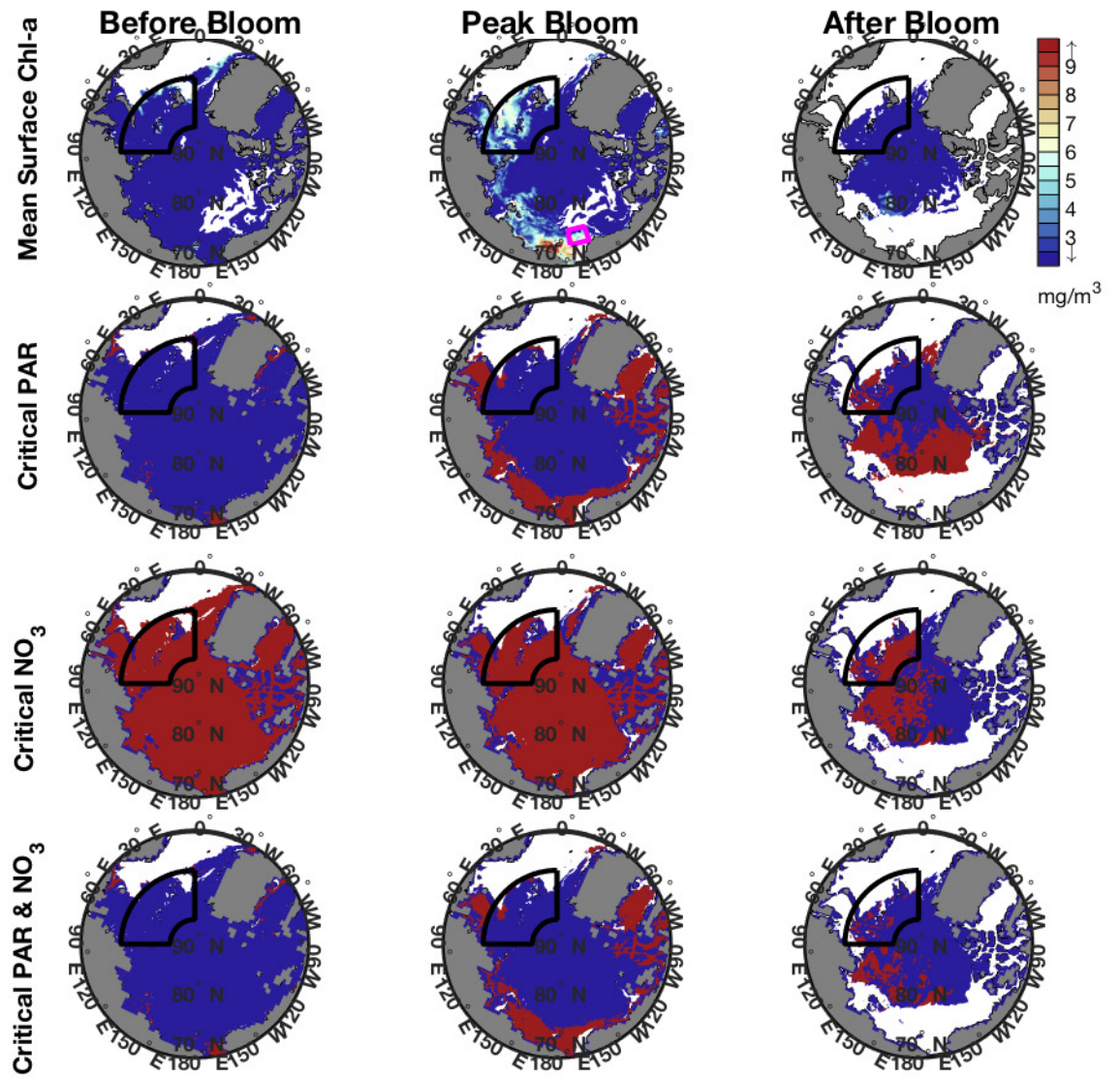
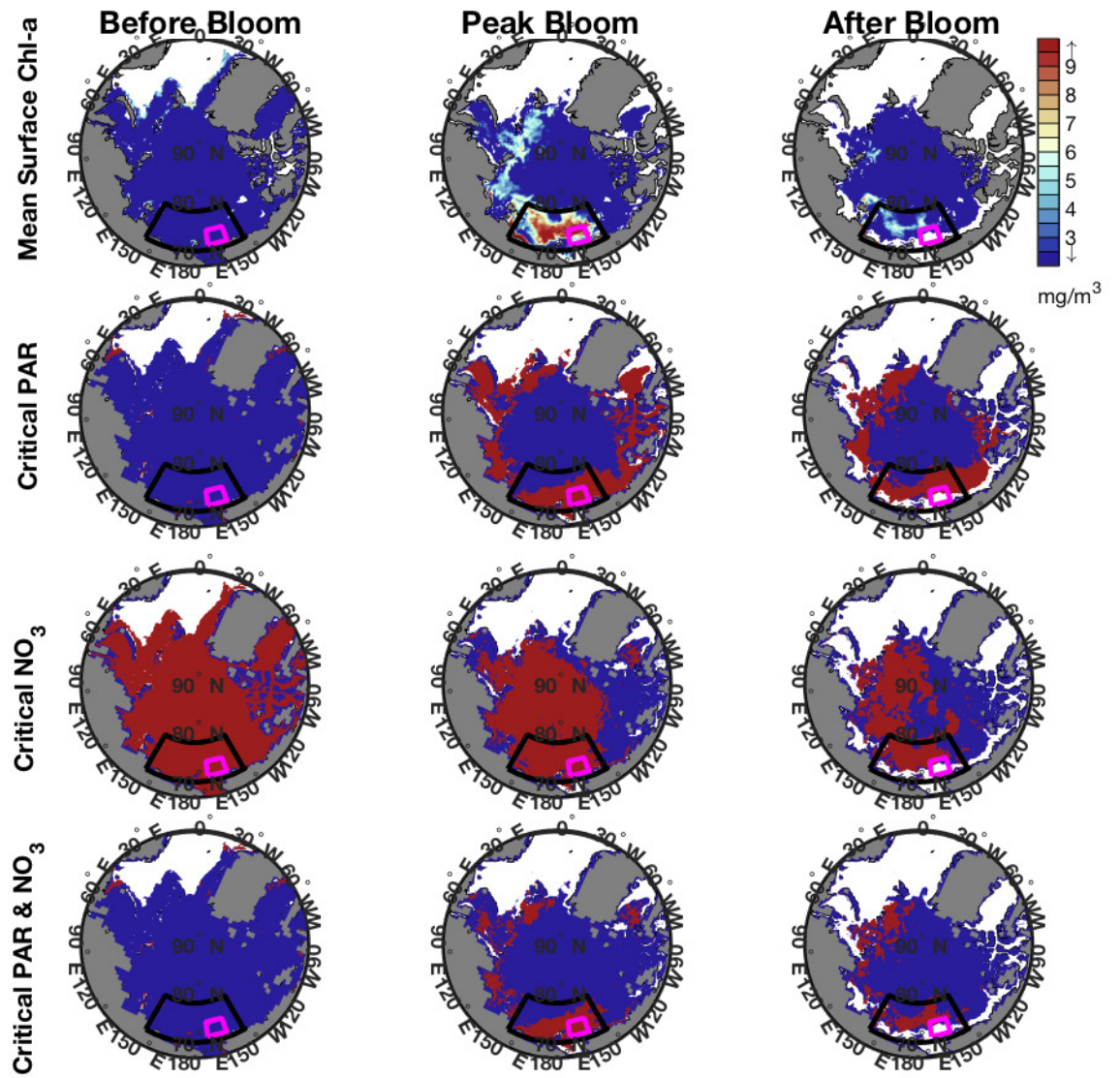


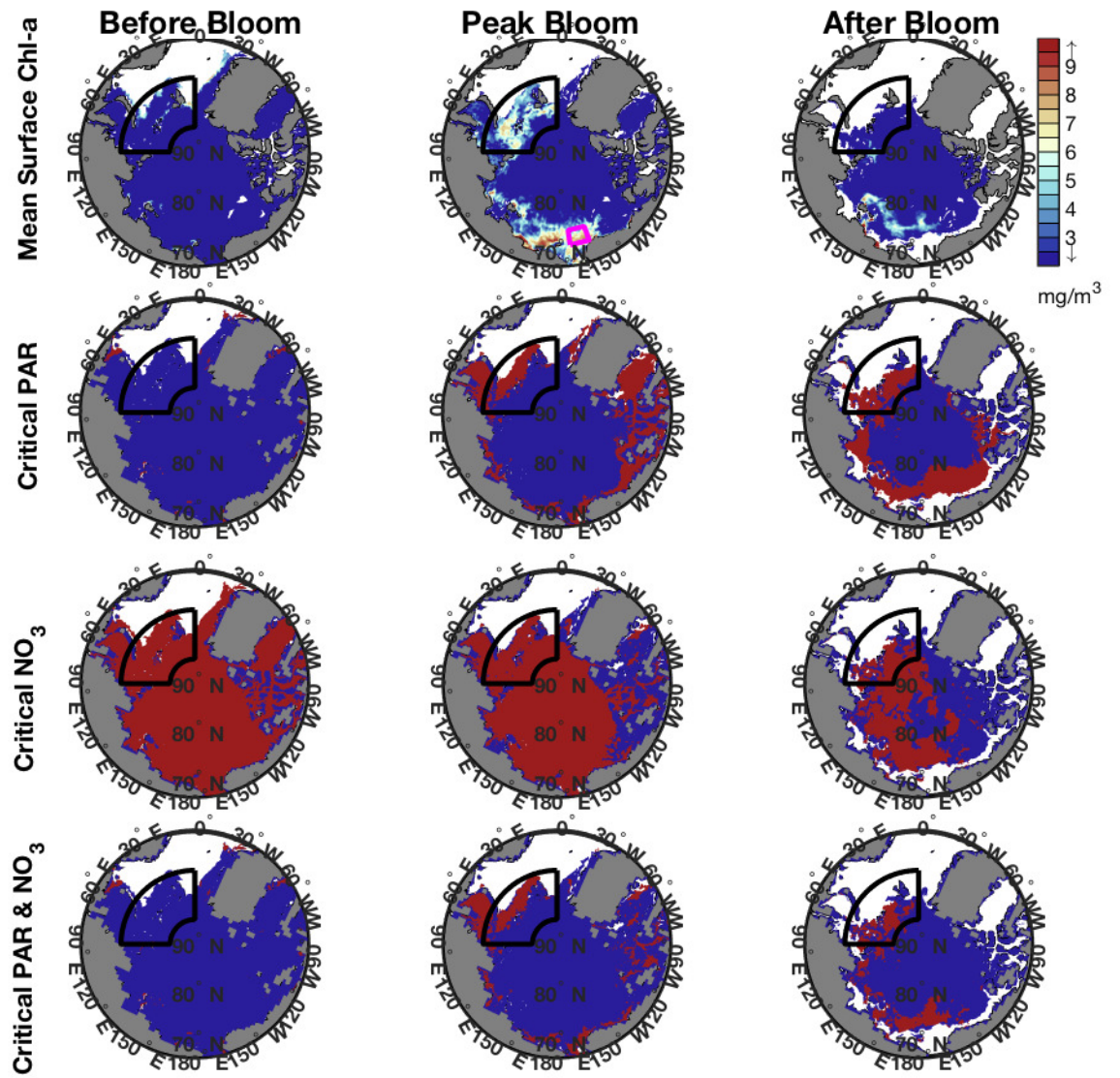
Figure 5. Same as in Figure 5, but for the Eastern Arctic Bloom.

388



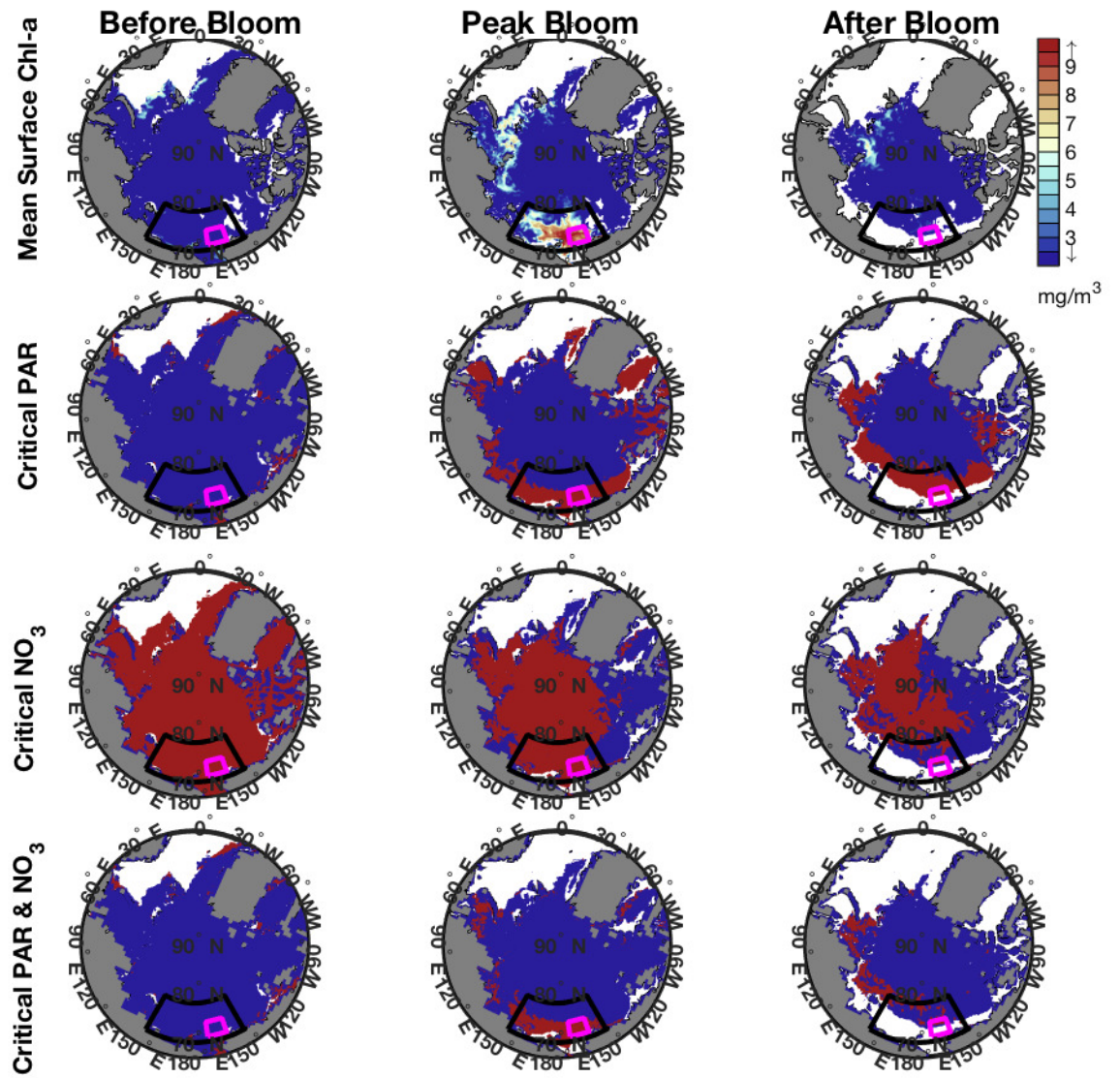
389

Figure 6. Same as in Figure 4, but for the Western Arctic Bloom in 2001



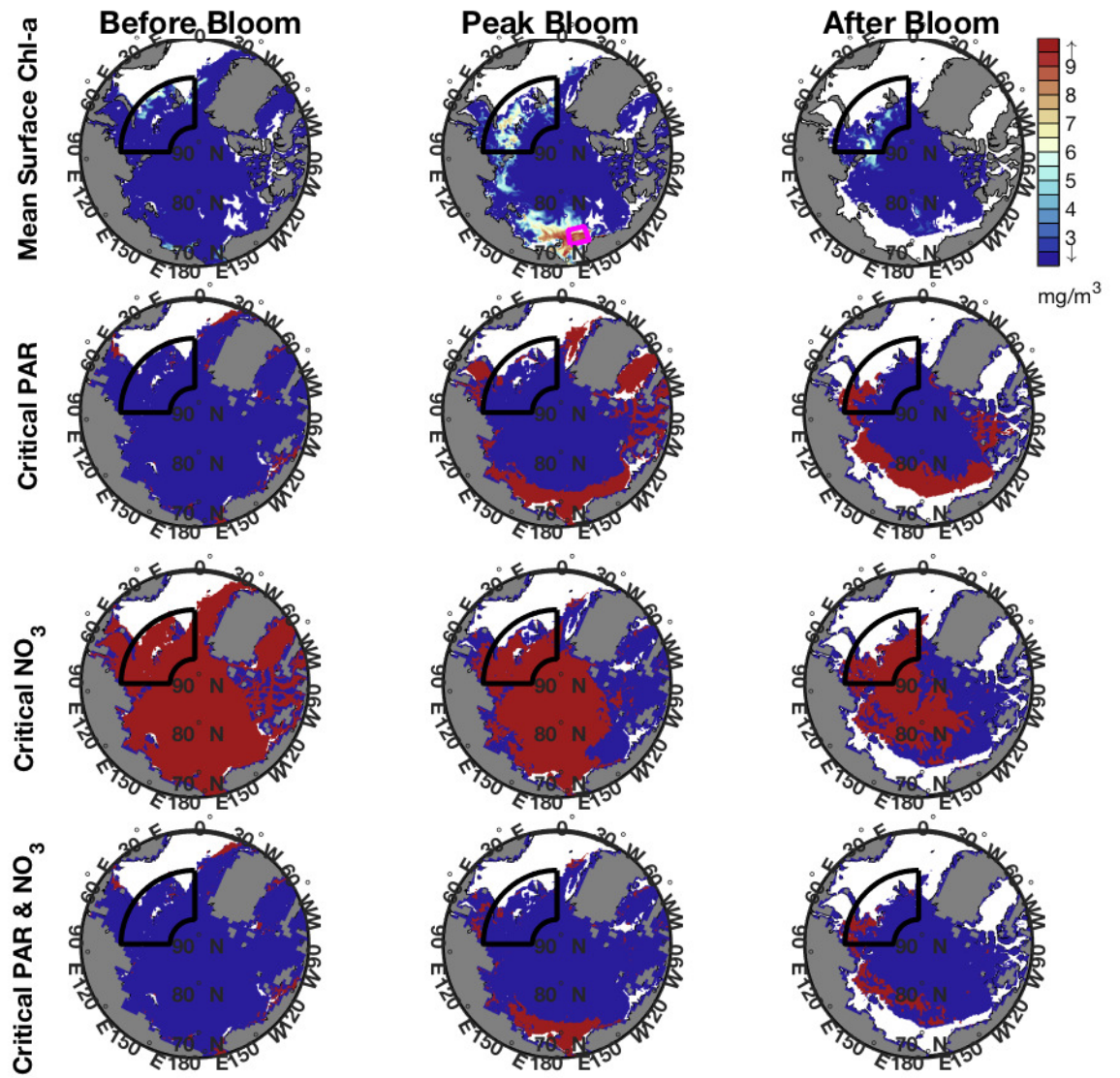
390

Figure 7. Same as in Figure 4, but for the Eastern Arctic Bloom in 2001



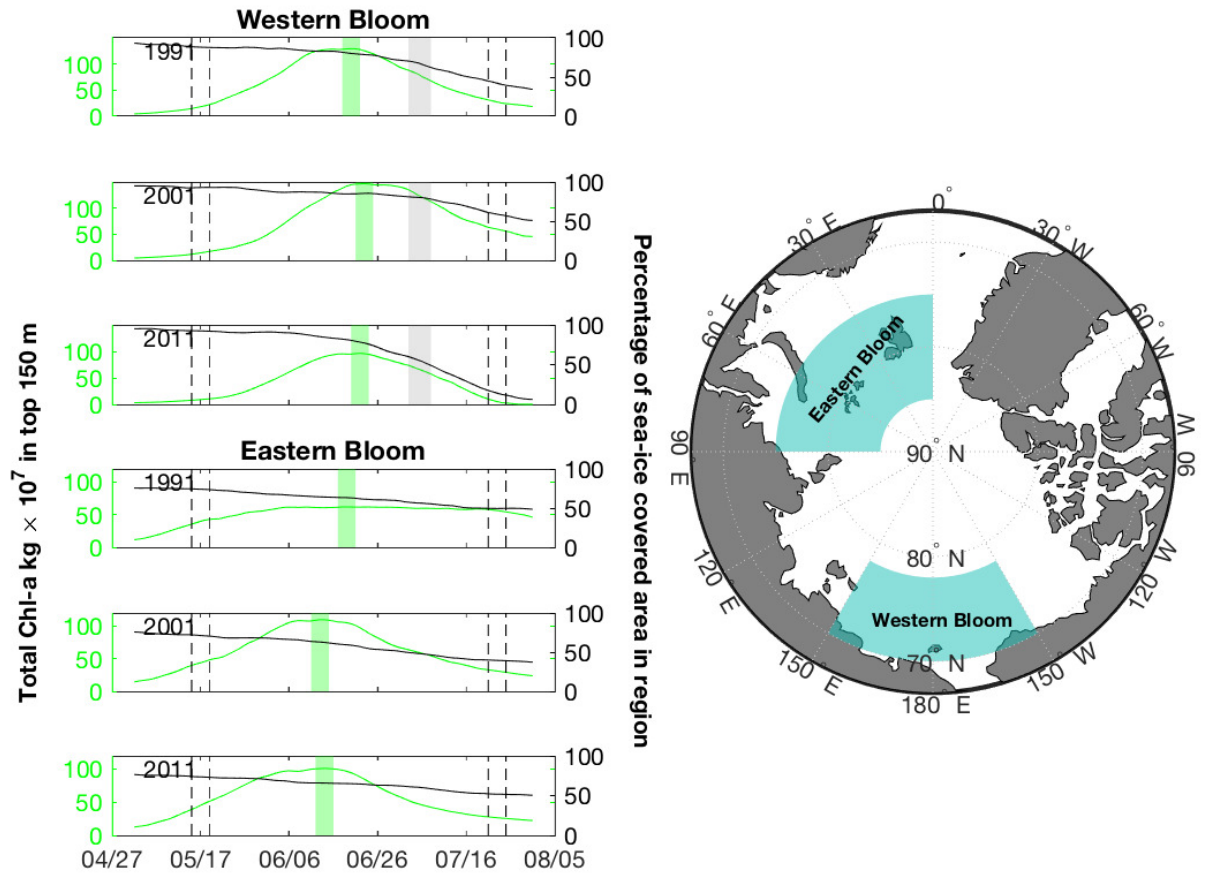
391

Figure 8. Same as in Figure 4, but for the Western Arctic Bloom in 1991

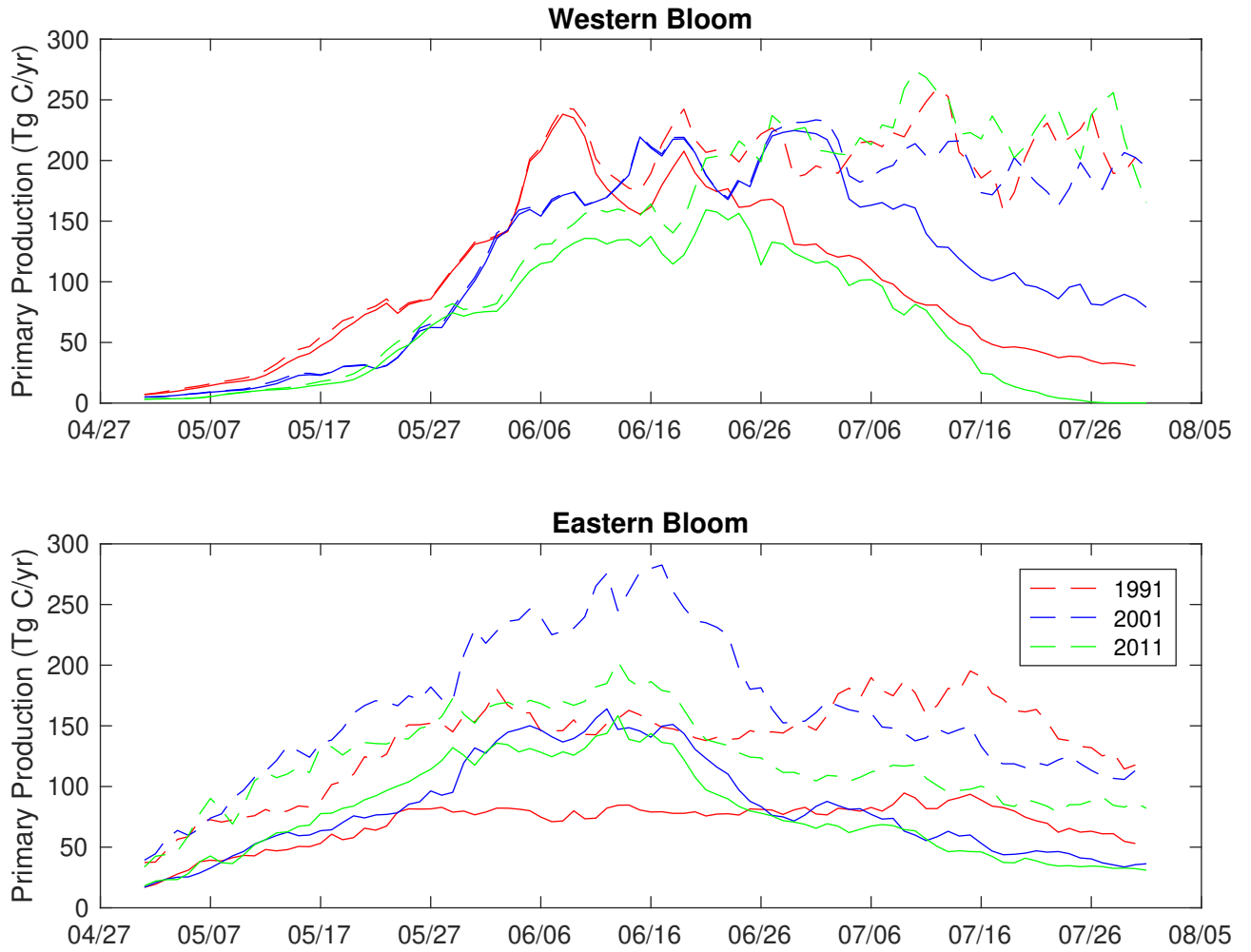


392

**Figure 9.** Same as in Figure 4, but for the Eastern Arctic Bloom in 1991.



393 **Figure 10.** Time series of spatially integrated surface chl-*a* (green lines) and percentage sea-  
 394 ice area (black lines) for the eastern and western under sea-ice bloom areas for the years 1991,  
 395 2001 and 2001. Vertical green bars delineate the 5-day period surrounding the date of the chl-*a*  
 396 maximum for each time series. Vertical gray bars delineate July 3-8 2011. Dashed lines indicate  
 397 the pre-bloom and post-bloom periods as shown in the first and last columns of Figures 4-9



398 **Figure 11.** Spatially-integrated model primary production for the WB and EB regions for  
 399 May, June and July of 1991, 2001 and 2001. Dashed lines represent primary production for the  
 400 entire region. Solid lines represent primary production for the portion of the region where ice  
 401 concentration is greater than 50%.